Journal of Power Sources 211 (2012) 59–65

Contents lists available at SciVerse ScienceDirect

Journal of Power Sources

journal homepage: www.elsevier.com/locate/jpowsour

# High rate micron-sized niobium-doped $LiMn_{1.5}Ni_{0.5}O_4$ as ultra high power positive-electrode material for lithium-ion batteries

Ting-Feng Yi [a,*], Ying Xie [b,**], Yan-Rong Zhu [a], Rong-Sun Zhu [a], Ming-Fu Ye [a]

[a] School of Chemistry and Chemical Engineering, Anhui University of Technology, Maanshan, Anhui 243002, PR China
[b] Key Laboratory of Functional Inorganic Material Chemistry, Ministry of Education, School of Chemistry and Materials Science, Heilongjiang University, Harbin 150080, PR China

ARTICLE INFO

*Article history:*
Received 6 March 2012
Accepted 29 March 2012
Available online 12 April 2012

*Keywords:*
Lithium-ion battery
Positive-electrode material
Spinel lithium manganese nickel oxide
Niobium doping
Rate-performance

ABSTRACT

Nb-doped $LiMn_{1.5}Ni_{0.5}O_4$ materials have been synthesized through a solid-state reaction, and Nb doping achieves some encouraging results. Both crystal domain size and electronic conductivity are influenced by this kind of doping. The lattice parameter of the Nb-doped $LiMn_{1.5}Ni_{0.5}O_4$ samples are slightly larger than that of pure $LiMn_{1.5}Ni_{0.5}O_4$ samples, and Nb doping does not change the basic spinel structure. Even though the material has a particle size of 1–2 μm, the capacity retention is improved remarkably compared to that of the undoped one when charge-discharged at high rates. The $LiNi_{0.525}Mn_{1.425}Nb_{0.05}O_4$ has a discharge capacity of 102.7 mAh $g^{-1}$ at 1 *C* charge–discharge rate after 100 cycles. Though all samples exhibit similar initial discharge capacities at various high C rates, the Nb-doped $LiMn_{1.5}Ni_{0.5}O_4$ samples display remarkable cyclabilities. Capacity retention of Nb-doped $LiMn_{1.5}Ni_{0.5}O_4$ is excellent without a significant capacity loss at various high C rates. This is ascribed to a smaller crystallite, a higher conductivity, and a higher lithium diffusion coefficient ($D_{Li}$) observed in this material. As a result, our microscale Nb-doped $LiMn_{1.5}Ni_{0.5}O_4$ can be used for battery applications that require high power and long life, including HEVs and energy storage devices for renewable energy systems.



## 1. Introduction

Rechargeable lithium-ion battery has a great potential as a new large-scale power source for plug-in hybrid vehicles (PHEVs) and electric vehicles (EVs) due to their high energy density, high voltage, and long cycle life. As we know, the current commercial lithium-ion batteries commonly based on layered Co oxide positive-electrode materials ($LiCoO_2$) can hardly fulfill the requirement of high power applications [1]. Thus, developing positive-electrode material with high energy density is one of the key challenges for lithium-ion batteries, which can be obtained either by high voltage or high capacity [2]. Since the pioneering work of K. Amine [3] in 1995, spinel $LiMn_{1.5}Ni_{0.5}O_4$ was found to be a particularly attractive positive-electrode material for lithium-ion batteries, because of its dominant potential plateau at around 4.7 V and high reversible capacity as well as its low cost and non-toxicity safety [4–7]. Hence, $LiMn_{1.5}Ni_{0.5}O_4$ has a higher energy density than that of $LiMn_2O_4$, and then makes it the most attractive material for practical use [8]. In addition, the energy density of $LiMn_{1.5}Ni_{0.5}O_4$ is 20% higher than that of $LiCoO_2$. Unfortunately, the cycling stability of the $LiMn_{1.5}Ni_{0.5}O_4$ positive electrode at high rates is not satisfactory. According to our previous review work [7], cation doping is considered as an effective way to improve the electrochemical performance of $LiMn_{1.5}Ni_{0.5}O_4$. The reported doping cations include $Mg^{2+}$ [9,10], $Cr^{3+}$ [11,12], $Co^{3+}$ [13], $Fe^{3+}$ [14], $Ti^{3+}$ [15,16], $Zr^{4+}$ [17], and $Ru^{4+}$ [18]. Various methods have been proposed to prepare $LiMn_{1.5}Ni_{0.5}O_4$, such as solid-state reaction [19], sol–gel [20], one-step precipitation method [21], molten salt [22], and so on. However, they have some other disadvantages, such as complicated synthetic routes and high synthetic cost, which is difficult for commercial applications. From a commercial viewpoint, the solid-state synthesis of $LiMn_{1.5}Ni_{0.5}O_4$ powders exhibits a potential commercial application due to the simple synthesis route and low synthesis cost. Our group reported that Nb doping can be considered as an effective way to improve the electrochemical performance of spinel $Li_4Ti_5O_{12}$ negative-electrode material [23]. To our knowledge, the rate cycling performance of Nb-doped $LiMn_{1.5}Ni_{0.5}O_4$ was not reported. It is well known that the structural change of spinel lithium manganese oxide ($LiMn_2O_4$) is due to the Jahn–Teller effect of $Mn^{3+}$ ions during cycles. Hence, we hope that there is no $Mn^{3+}$ ion in our synthesized product. During

* Corresponding author. Tel.: +86 555 2311807; fax: +86 555 2311552.
** Corresponding author.
*E-mail addresses:* tfyihit@163.com (T.-F. Yi), xieying@hlju.edu.cn (Y. Xie).

0378-7753/$ – see front matter © 2012 Elsevier B.V. All rights reserved.
doi:10.1016/j.jpowsour.2012.03.095

charge–discharge of $LiMn_{1.5}Ni_{0.5}O_4$, the change of nickel valence state occurs as follows:

$$Li\left[Mn_{1.5}^{4+}Ni_{0.5}^{2+}\right]O_4 \underset{\text{Discharge}}{\overset{\text{Charge}}{\rightleftharpoons}} \left[Mn_{1.5}^{4+}Ni_{0.5}^{4+}\right]O_4 + Li^+ + e^- \quad (1)$$

According to the equation mentioned above, the charge–discharge capacity of $LiMn_{1.5}Ni_{0.5}O_4$ is from the reversible redox reactions between bivalent nickel ion ($Ni^{2+}$) and tetravalent nickel ion ($Ni^{4+}$). The more the $Ni^{2+}$ that exists in $LiMn_{1.5}Ni_{0.5}O_4$, the more lithium ions can deintercalate from the host, so the more lithium ions can intercalate into the anode, and increase the discharge capacity. Hence, Nb-doped $LiMn_{1.5}Ni_{0.5}O_4$ compound ($LiMn_{1.425}Ni_{0.525}Nb_{0.05}O_4$ and $LiMn_{1.425}Ni_{0.4}Nb_{0.1}O_4$) was prepared by a solid-state method. The electrochemical performances of Nb-doped $LiMn_{1.5}Ni_{0.5}O_4$, including cycling stability and rate capability, were extensively evaluated in half cells.

## 2. Experimental

### 2.1. Material preparation

The Nb-doped powder samples were prepared by a solid-state method. A mixture of $MnO_2$, $Li_2CO_3$, NiO and $Nb_2O_5$ in proper amount was mixed by ball milling for 5 h in an acetone slurry, followed by drying at 80 °C for 12 h. Then, the powders were calcined at 850 °C for 24 h in a flowing air atmosphere to obtain the samples.

### 2.2. Material characterization

Differential thermal analysis (DTA) and thermogravimetry (TG) measurements were performed in air from room temperature to 800 °C with a Henjiu Chare Tianping-1/2 thermal analysis system (Beijing, China) under a scanning rate of 5 °C $min^{-1}$. XRD was performed on Rigaku D/MAX-2400 X-ray diffractometer with Cu $K\alpha_1$ ($10° < 2\theta < 80°$) monochromated radiation in order to identify the crystalline phase. The particle morphologies were examined with a scanning electron microscope (Hitachi, S-4000). Charge–discharge performance was characterized galvanostatically on Land 2000T (China) tester at 0.1 *C* charge rate and 1, 3 and 5 *C* discharge rates between 3.3 and 4.95 V (vs. $Li/Li^+$), respectively. Cyclic voltammograms of both electrodes ware measured on an electrochemical workstation (CHI 852C) between 3.3 and 5 V (vs. $Li/Li^+$). EIS measurements were carried out in two-electrode cells by using Zahner Zennium IM6ex electrochemical workstation with a ±5 mV ac signal and a frequency range from $10^4$ to 0.1 Hz. The prepared positive-electrode materials were adopted as the work electrode; the counter electrode and reference electrode were Li foil.

### 2.3. Battery preparation

The electrode was prepared by pasting a slurry containing 80 wt % active material, 10 wt% carbon black, and 10 wt% polyvinylidene fluoride dissolved in *N*-methylpyrroline onto a Al foil. After coating, the film was dried in a vacuum oven at 100 °C for 12 h, and then cut into a sheet. Before using, the sheet was dried in a vacuum chamber at 120 °C for 10 h. Two-electrode batteries for cycles were assembled in an Ar-filled glove box using a metal lithium foil as counter electrode, 1 M $LiPF_6$ in a 1:1 (v/v) mixture of ethylene carbonate (EC) and dimethyl carbonate (DMC) as electrolyte and Celgard 2300 polypropylene as separator.

## 3. Results and discussion

Fig. 1a and b shows the TG–DTA curves of $LiMn_{1.5}Ni_{0.5}O_4$, $LiMn_{1.425}Ni_{0.525}Nb_{0.05}O_4$ obtained from the ternary precursors of $MnO_2$, $Li_2CO_3$, NiO and $Nb_2O_5$. There are two temperature intervals where significant mass loss can be detected. The first one is the interval between room temperature and about 220 °C, which may be due to the removal of moisture and entrapped water [24,25]. In the second region (300–520 °C), the endothermic peak observed

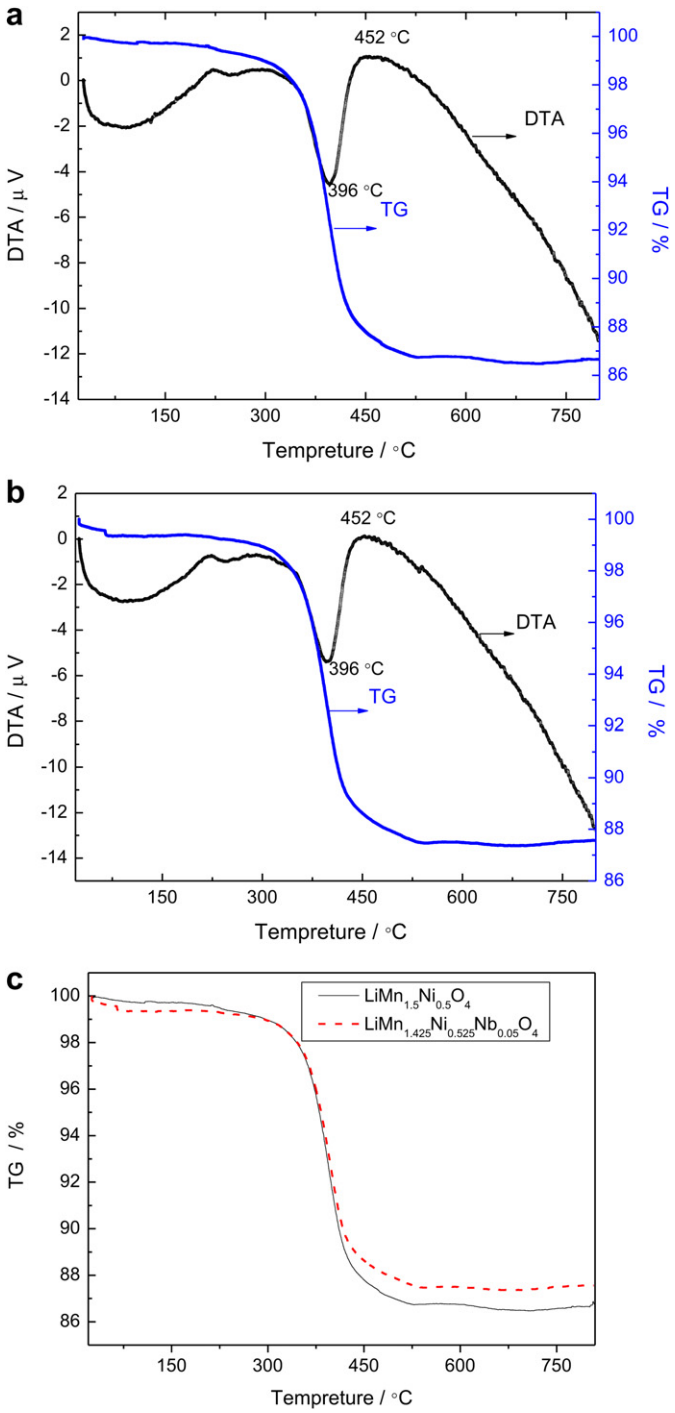


**Fig. 1.** TG–DTA curves for the thermal decomposition of the precursors of (a) $LiMn_{1.5}Ni_{0.5}O_4$ and (b) $LiMn_{1.425}Ni_{0.525}Nb_{0.05}O_4$; (c) TG curves for the thermal decomposition of the precursors of $LiMn_{1.5}Ni_{0.5}O_4$ and $LiMn_{1.425}Ni_{0.525}Nb_{0.05}O_4$.

at 396 °C is accompanied by noticeable weight lose in the TG curve. It can be considered as a result of the decomposition of the inorganic constituents of the precursor followed by crystallization of spinel phase. In addition, it can be clearly seen an exothermic peaks located at around 452 °C in the DTA curves. This can be assigned to the phase-change reaction, the formation of $LiMn_{1.5}Ni_{0.5}O_4$ or $LiMn_{1.425}Ni_{0.525}Nb_{0.05}O_4$, and the completion of the crystallization reaction. It corresponds to the following reaction

$$Li_2CO_3 + NiO + 3MnO_2 = 2LiMn_{1.5}Ni_{0.5}O_4 + CO_2 \quad (2)$$

$$Li_2CO_3 + 1.05NiO + 2.85MnO_2 + 0.05Nb_2O_5 = 2LiMn_{1.425}Ni_{0.525}Nb_{0.05}O_4 + CO_2 \quad (3)$$

In the last region, the TG curve becomes flat and no sharp peaks can be observed in the DTA curve, indicating that no phase transformation occurs, and that any further heating only makes the structure of samples more perfectly. Fig. 1a and b indicates that the Nb doping does not change the reaction mechanism and the phase transition reaction. From Fig. 1c, it can be seen that the weight loss of Nb-doped $LiMn_{1.5}Ni_{0.5}O_4$ is lower than that of pristine $LiMn_{1.5}Ni_{0.5}O_4$. The reason is that the former has a larger molar mass than that of the latter.

XRD patterns of substituted and unsubstituted $LiMn_{1.5}Ni_{0.5}O_4$ samples are shown in Fig. 2, and the inset shows the enlarged (1 1 1) peaks. All of the diffraction peaks are assigned to the spinel compound $LiMn_{1.5}Ni_{0.5}O_4$. This means that the low dose doping of $Nb^{5+}$ cannot change the basic $LiMn_{1.5}Ni_{0.5}O_4$ structure, and form a solid solution. The crystal structure of $LiMn_{1.5}Ni_{0.5}O_4$ is plotted in Fig. 3. $Li^+$ ions occupy the tetrahedral (8a) sites; Mn or Ni ions reside at the octahedral (16d) sites random; and $O^{2-}$ ions are located at (32e) sites. The full width at half maximum (FWHM) values of the (3 1 1) and (4 0 0) diffraction lines of Nb-doped $LiMn_{1.5}Ni_{0.5}O_4$ samples are larger those of $LiMn_{1.5}Ni_{0.5}O_4$. It can be concluded that the atom location confusion appears in the Nb-doped $LiMn_{1.5}Ni_{0.5}O_4$, for example, some lithium atom or metal ions (Mn, Ni and Nb) are exchanged to form anti-spinel structure because of the Nb doping [26,27]. In addition, small NiO impurity peak can be found at 44 and 63–64° in the two theta range as shown in Fig. 2, suggesting an oxygen loss reaction at high temperatures. The reason is that $LiMn_{1.5}Ni_{0.5}O_4$ losses oxygen and disproportionates to a spinel and rock salt NiO when it is heated

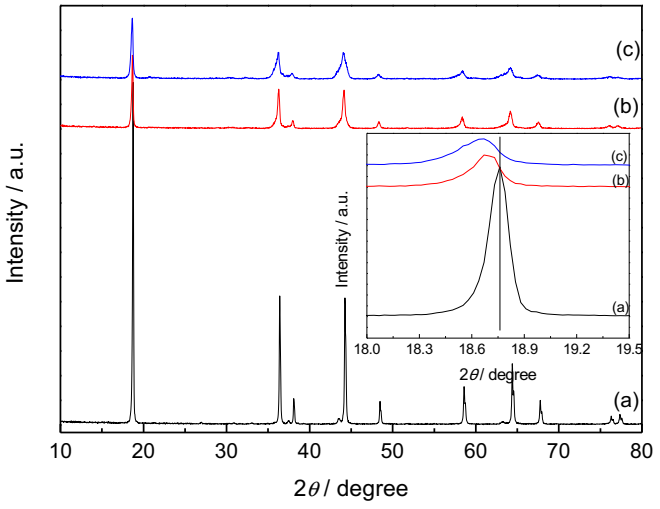


**Fig. 2.** Powder XRD patterns of (a) $LiNi_{0.5}Mn_{1.5}O_4$, (b) $LiMn_{1.425}Ni_{0.525}Nb_{0.05}O_4$ and (c) $LiMn_{1.425}Ni_{0.4}Nb_{0.1}O_4$. Inset shows the enlarged (111) peaks for the Nb-doped $LiNi_{0.5}Mn_{1.5}O_4$ materials.

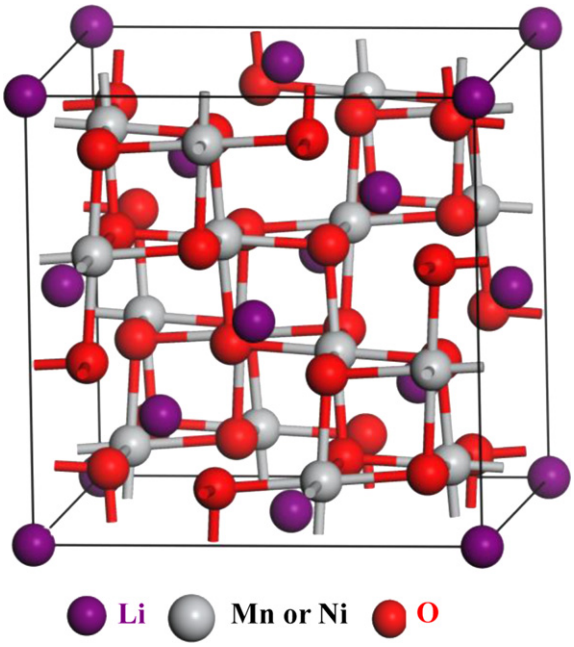


**Fig. 3.** Crystal structure of $LiMn_{1.5}Ni_{0.5}O_4$. $Li^+$ ions occupy the tetrahedral (8a) sites; Mn or Ni ions reside at the octahedral (16d) sites random; and $O^{2-}$ ions are located at (32e) sites.

above 600 °C [28]. The formation of the NiO impurity phase can be shown by the generalized reaction:

$$LiMn_{1.5}Ni_{0.5}O_4 \rightarrow \alpha NiO + \beta LiMn_{1.5+x}Ni_{0.5-x}O_4 + \gamma O_2 \quad (4)$$

where $\alpha$, $\beta$ and $\gamma$ define, respectively, the relative amounts of the NiO, $LiNi_{0.5-x}Mn_{1.5+x}O_4$, and $O_2$ phase. There is a slight shift in the diffraction peaks to the lower $2\theta$ values for the sample Nb-doped $LiMn_{1.5}Ni_{0.5}O_4$ compared to pure $LiMn_{1.5}Ni_{0.5}O_4$. This fact indicates that the lattice parameters of the Nb-doped $LiMn_{1.5}Ni_{0.5}O_4$ materials are slightly larger than that for the pure $LiMn_{1.5}Ni_{0.5}O_4$. These variations are attributed to the ionic radius differences among $Li^+$ (0.59 Å), $Ni^{2+}$ (0.69 Å), $Mn^{4+}$ (0.53 Å), and $Nb^{5+}$ (0.64 Å) [29]. The lattice parameters were calculated through the least square program method from the diffraction data of $LiMn_{1.425}Ni_{0.525}Nb_{0.05}O_4$ and $LiMn_{1.425}Ni_{0.4}Nb_{0.1}O_4$, and were found to be about 8.225 and 8.230 Å, respectively, which is slightly larger than that of a pristine $LiMn_{1.5}Ni_{0.5}O_4$ positive-electrode material (8.186 Å). The expansile channels reduce the block for the diffusion of $Li^+$, and then improve the electrochemical performance of the material. Ohzuku et al. [30] reported that any occupancy of the substituent ions in the 8a tetrahedral lithium sites will lead to unfavorable electrochemical characteristics. According to Ohzuku et al. [30], the integrated intensity ratios of the (4 0 0)/(3 1 1) peaks are indices of the extent of occupancy of the substituent ions in the 8a lithium sites. The intensity ratios of the (4 0 0)/(3 1 1) peaks for pristine $LiMn_{1.5}Ni_{0.5}O_4$, $LiMn_{1.425}Ni_{0.525}Nb_{0.05}O_4$ and $LiMn_{1.425}Ni_{0.4}Nb_{0.1}O_4$ are 0.985, 0.976 and 0.996, respectively. The integrated intensity ratio of the (4 0 0)/(3 1 1) for $LiMn_{1.425}Ni_{0.4}Nb_{0.1}O_4$ increases compared to $LiMn_{1.5}Ni_{0.5}O_4$. This suggests that nickel shows a propensity to occupy the 8a lithium sites in $LiMn_{1.425}Ni_{0.4}Nb_{0.1}O_4$ due to the NiO impurity. Hence, it is important that a proper Nb doping level should be optimized to achieve a good cell performance.

SEM images of as-prepared Nb-doped $LiMn_{1.5}Ni_{0.5}O_4$ samples are shown in Fig. 4. All samples exhibit the highly crystalline particles with a particle size in the range of 1–2 μm, and the $Nb^{5+}$ substitution to some extent reduce the particle size of $LiMn_{1.5}Ni_{0.5}O_4$. The small

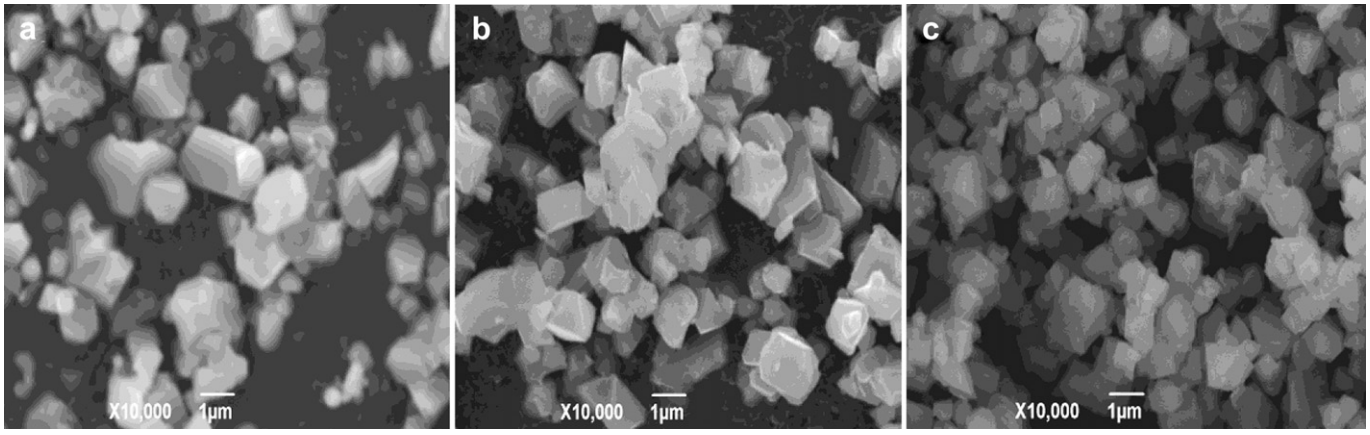


**Fig. 4.** SEM micrographs of (a) $LiMn_{1.5}Ni_{0.5}O_4$, (b) $LiMn_{1.425}Ni_{0.525}Nb_{0.05}O_4$ and (c) $LiMn_{1.425}Ni_{0.4}Nb_{0.1}O_4$.

particle size results in sufficient contact between active materials and electrolyte and results in favorable diffusion and transmission of $Li^+$ in the electrode.

Fig. 5 shows cyclic voltammograms of $LiMn_{1.5}Ni_{0.5}O_4$ and $LiMn_{1.425}Ni_{0.525}Nb_{0.05}O_4$ electrodes at a scanning rate of 0.1 mV $s^{-1}$. The redox peaks mainly located near 4.7 V are ascribed to the two-step oxidation/reduction of $Ni^{2+}/Ni^{4+}$ [31] or $Ni^{2+}/Ni^{3+}$ and $Ni^{3+}/Ni^{4+}$ [32], and small redox peaks appear near 4.0 V can be attributed to the redox reaction of $Mn^{3+}/Mn^{4+}$ couples. The much smaller difference in potential between the anodic and cathodic peaks in $LiMn_{1.425}Ni_{0.525}Nb_{0.05}O_4$ compared to that in $LiMn_{1.5}Ni_{0.5}O_4$ suggests faster lithium insertion/extraction kinetics in the former. This observation confirms that the Nb doping enhances the reversibility of the $LiMn_{1.5}Ni_{0.5}O_4$, indicating that Nb-doped electrode has good reversibility and good rate capability.

To investigate the possible reason of improved cycling performance of the Nb-doped $LiMn_{1.5}Ni_{0.5}O_4$, electrochemical impedance spectroscopy (EIS) was measured before cycling in Fig. 6, and a possible equivalent circuit was inserted in Fig. 6. In this equivalent circuit, $R_s$ represents the ohmic resistance; $R_f$ and $C_f$ (the first $Q$) are, respectively, the resistance and capacitance of a solid electrolyte interphase (SEI) film, and $W$ is the Warburg impedance of solid-phase diffusion. $R_{ct}$ and $C_{dl}$ represent the charge-transfer resistance and double layer capacitance for lithium-ion intercalation, respectively [33,34]. It can be seen from Fig. 6 that the $R_S$ values of different samples are almost constant, whereas $R_{ct}$ values vary greatly with different samples. The difference of $R_S$ values between two samples may be caused by the simulated errors. The $R_{ct}$ of the $LiMn_{1.5}Ni_{0.5}O_4$ sample is found to be much higher than that of the $LiMn_{1.425}Ni_{0.525}Nb_{0.05}O_4$ sample due to the Nb doping, indicating that the latter has a much better conductivity than the former. The minimum $R_{ct}$ value of $LiMn_{1.425}Ni_{0.525}Nb_{0.05}O_4$ means a lower electrochemical polarization, and this can lead to higher rate cycling performance.

The diffusion coefficient ($D_{Li}$) of lithium ion can be calculated from the plots in the low-frequency region. The equation for the calculation of $D_{Li}$ values by EIS can be expressed as [35,36]:

$$Z_{re} = R_{ct} + R_s + \sigma\omega^{-0.5} \quad (5)$$

$$D_{Li} = \frac{(RT)^2}{2(An^2F^2C_{Li}\sigma)^2} \quad (6)$$

where the meanings of $T$ is the absolute temperature, $R$ the gas constant, $n$ the number of electrons per molecule during oxidization, $A$ the surface area, $F$ the Faraday's constant, $C_{Li}$ the concentration of lithium ion, $\omega$ the angular frequency, and $\sigma$ is the Warburg factor which has relationship with $Z_{re}$. The $Z_{re} - \omega^{-1/2}$ plots were presented in Fig. 7. A linear characteristic could be

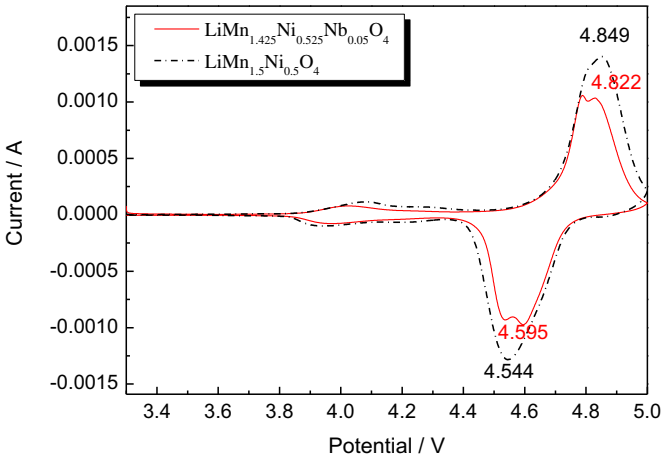


**Fig. 5.** Cyclic voltammograms of $LiMn_{1.5}Ni_{0.5}O_4$ and $LiMn_{1.425}Ni_{0.525}Nb_{0.05}O_4$ cells between 3.3 and 5 V with a scanning rate 0.1 mV $s^{-1}$.

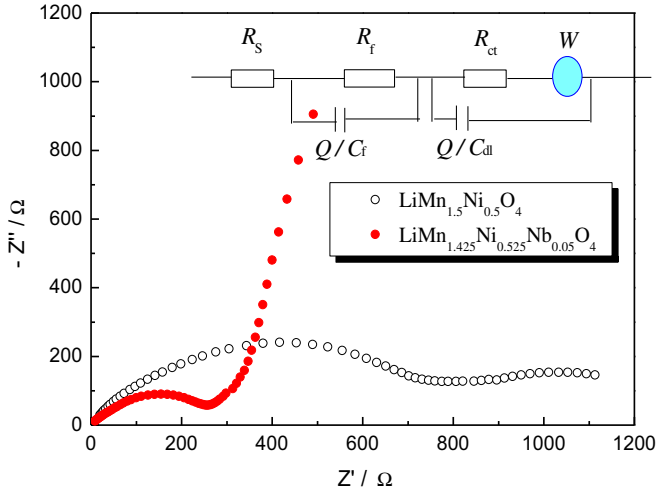


**Fig. 6.** Nyquist plots of $LiMn_{1.5}Ni_{0.5}O_4$ and $LiMn_{1.425}Ni_{0.525}Nb_{0.05}O_4$ electrodes. Inset is the selected equivalent circuit.

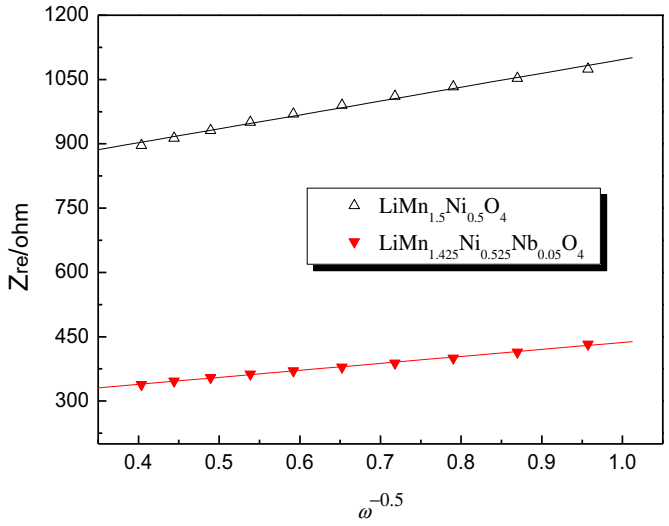


**Fig. 7.** $Z'$ *vs.* $\omega^{-0.5}$ plots in the low-frequency region obtained from EIS measurements.

seen for both curves. According to Eqs. (5) and (6), the lithium diffusion coefficients of $LiMn_{1.5}Ni_{0.5}O_4$ and $LiMn_{1.425}Ni_{0.525}Nb_{0.05}O_4$ are calculated to be approximate $2.55 \times 10^{-16}$ and $10.07 \times 10^{-16}$ $cm^2\ s^{-1}$, respectively. It is clear that the diffusion coefficient of lithium ion is greatly increased due to the Nb doping. This suggests that Nb-doping contributes to the enhancement of ionic conductivity, and is favorable for migrating lithium ion and maintaining stable crystal structure.

The initial discharge and consecutive charge profiles at 0.1 *C* charge rates and 1 *C* discharge rates for the sample $LiMn_{1.5}Ni_{0.5}O_4$, $LiMn_{1.425}Ni_{0.525}Nb_{0.05}O_4$ and $LiMn_{1.425}Ni_{0.4}Nb_{0.1}O_4$ are given in Fig. 8. Their initial discharge capacities are 114.9, 116.7 and 109.4 mAh $g^{-1}$, respectively. All discharge and charge curves exhibit two potential plateaus at 4.0 and 4.7 V, revealing that the doping cannot change the basic spinel structure. In addition, Nb-doped $LiMn_{1.5}Ni_{0.5}O_4$ materials have a higher discharge plateau at about 4.7 V than that of pure $LiNi_{0.5}Mn_{1.5}O_4$, indicating that Nb-doped $LiMn_{1.5}Ni_{0.5}O_4$ materials have a higher power density than that of pure $LiMn_{1.5}Ni_{0.5}O_4$. Fig. 8b–d also gives the cycling performance profiles of the substituted and unsubstituted $LiMn_{1.5}Ni_{0.5}O_4$ samples at various high C rates. The cell was charged using a current density of 0.1 *C* rate before each discharge test. All samples exhibit similar initial discharge capacities at various high C rates, but the Nb-doped $LiMn_{1.5}Ni_{0.5}O_4$ samples display remarkable cyclability without much fade at various high C rates compared to the drastic fade seen with the $LiMn_{1.5}Ni_{0.5}O_4$ sample. These may be explained by the facts that: (1) smaller particles (see Fig. 4) can provide more interfacial area for contact within the liquid electrolyte and, hence, can increase the opportunity for lithium ions to intercalate back the host structure [37]; (2) Nb-doping decreases

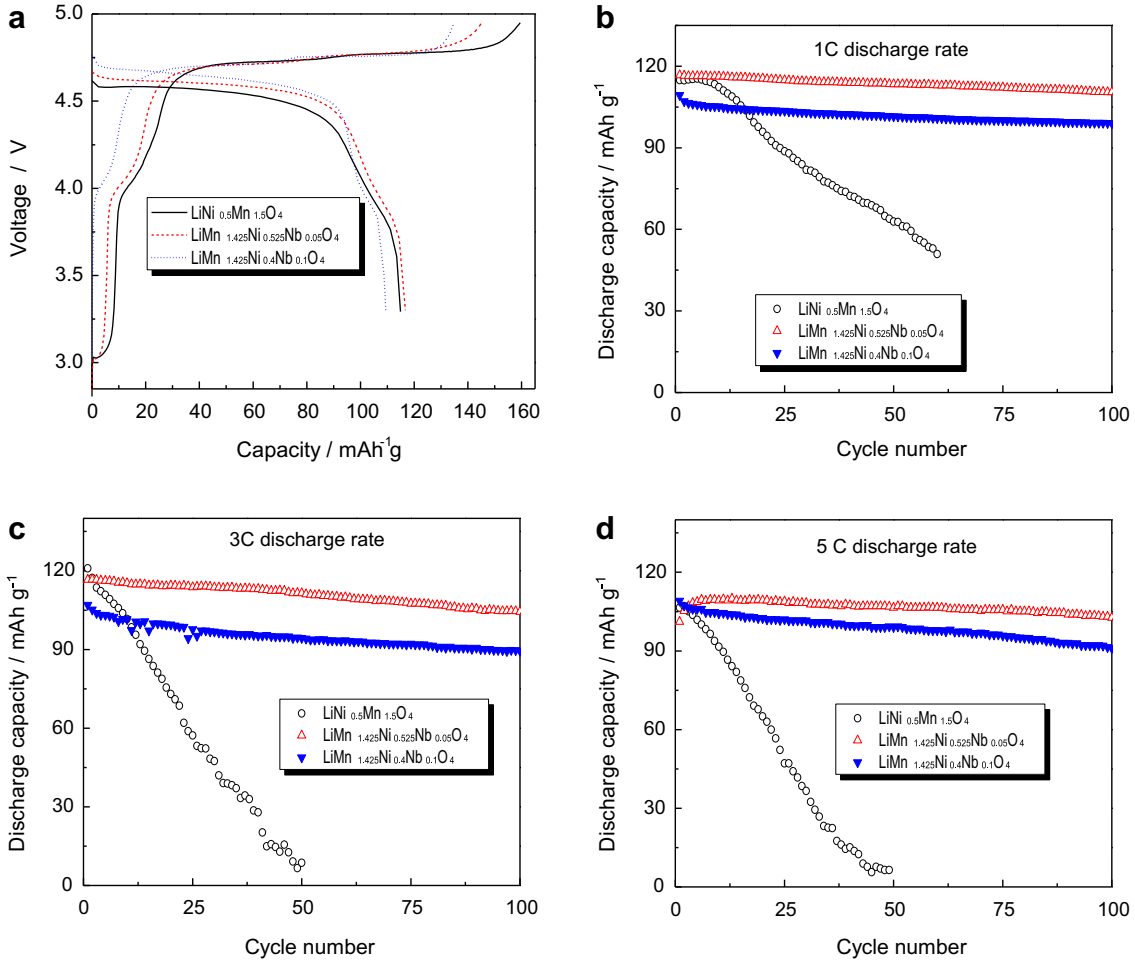


**Fig. 8.** (a) Initial charge–discharge curves (0.1 *C* charge rate and 1 *C* discharge rate) and cycling performance at (b) 1 *C* discharge rate, (c) 3 *C* discharge rate, and (d) 5 *C* discharge rate of $LiNi_{0.5}Mn_{1.5}O_4$ with and without Nb doping.

the charge-transfer resistance, and then increase the electronic conductivity (see Fig. 6); (3) the migration ability of lithium ion and reversibility (see Fig. 5)are greatly improved due to the Nb doping, and then the kinetics of $Li^+$ intercalation/de-intercalation and electron transfer are enhanced.

High voltage, portability, safety and excellent cyclability contribute to the commercial success of lithium-ion batteries [38]. As we know, the fast charge–discharge is very important during the practical commercial application. To provide more information about the electrochemical performances of the Nb-doped $LiMn_{1.5}Ni_{0.5}O_4$, the cycling performance and the coulomb efficiency of $LiMn_{1.425}Ni_{0.525}Nb_{0.05}O_4$ charge–discharged at 1 *C* rate in the voltage range of 3.3–4.95 V is given in Fig. 9. An interesting thing is that the discharge capacity increases slightly in the initial stage and the electrode reaches a largest discharge capacity after several cycles as shown in Fig. 9. The reason may be that the $LiMn_{1.425}Ni_{0.525}Nb_{0.05}O_4$ electrode is not thoroughly wetted by the electrolyte due to the fast charge–discharge. As shown in Fig. 9, after 100 cycles, the discharge capacity of the $LiMn_{1.425}Ni_{0.525}Nb_{0.05}O_4$ still remains near 100% of original values, indicating a high utility of electric capability. This efficiency is defined as the discharge capacity divided by the charge capacity in one charge/discharge cycle. It is interesting that the coulombic efficiencies of $LiMn_{1.425}Ni_{0.525}Nb_{0.05}O_4$ in the first charge–discharge cycle is about 89%, indicating that a small fraction of lithium ions is incapable of intercalating back into the host structure due to electrolyte decomposition at high voltage. However,

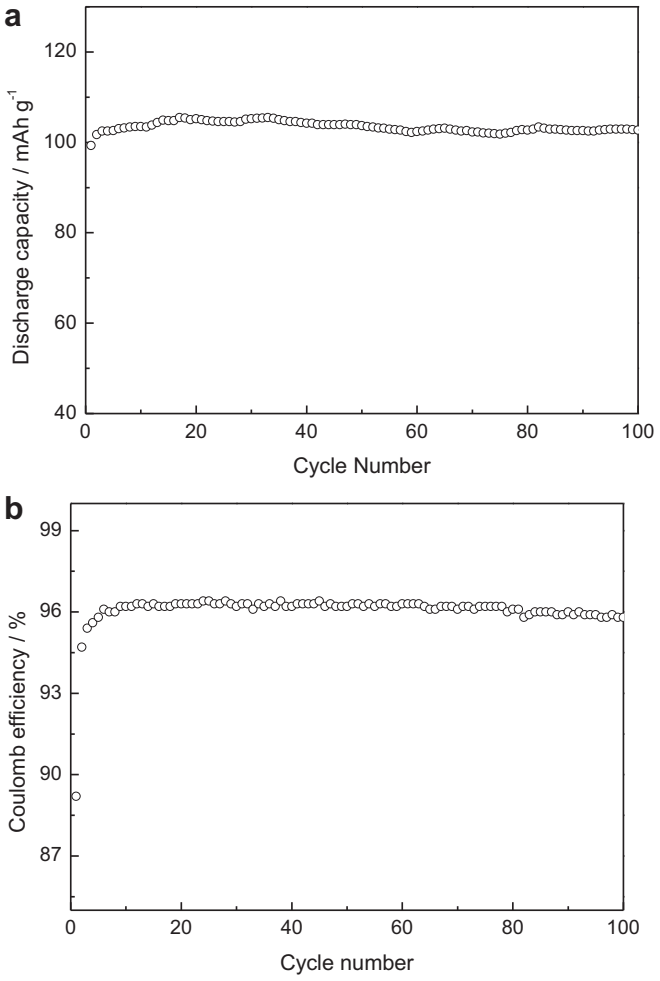


**Fig. 9.** (a) Capacity *vs.* cycle number and (b) coulombic efficiency of $LiMn_{1.425}Ni_{0.525}Nb_{0.05}O_4$ charge–discharged 1 *C* rate between 3.3 and 4.95 V.

after about two cycles, the coulomb efficiencies are increased to nearly a constant value (more than 96%). The improved cycling efficiency may be attributed to the formation of protective layer on the electrode surface after the first charge–discharge process. The mean coulombic efficiency of $LiMn_{1.425}Ni_{0.525}Nb_{0.05}O_4$ (about 96%) charge–discharged at 1 *C* is higher that that of $LiMn_{1.4}Cr_{0.2}Ni_{0.4}O_4$ electrode (about 94%) charge–discharged at 0.15 *C* reported by our previous work [39]. This result implies that Nb substitution is beneficial to the reversible intercalation and deintercalation of $Li^+$. The $LiMn_{1.425}Ni_{0.525}Nb_{0.05}O_4$ is characterized by an excellent rechargeability in terms of capacity retention, whereas it is well known that $LiMn_{1.5}Ni_{0.5}O_4$ batteries are normally primary or can be cycled only a limited number of times. $LiMn_{1.425}Ni_{0.525}Nb_{0.05}O_4$ can be environmentally friendly, reliable, safe, and low-cost power sources applied in occasions in which both high energy and power densities are necessary.

## 4. Conclusions

Nb-doped $LiMn_{1.5}Ni_{0.5}O_4$ positive-electrode materials were prepared by a solid-state synthetic method, and the structure and electrochemical performance were studied by TG–DTA, XRD, SEM, CV, EIS and galvanostatic charge–discharge test. The result shows that Nb doping achieves some encouraging results. Both crystal domain size and electronic conductivity are influenced by this kind of doping. This high voltage $LiMn_{1.425}Ni_{0.525}Nb_{0.05}O_4$ material presents good capacity retention of 110.5 mAh $g^{-1}$ at 1 C and 102.7 mAh $g^{-1}$ at 5 *C* discharge rate (0.1 *C* charge rates). Nb-doped $LiMn_{1.5}Ni_{0.5}O_4$ samples display remarkable cyclability without much fade at various high C rates compared to the drastic fade seen with the $LiMn_{1.5}Ni_{0.5}O_4$ sample. Nb-doped $LiMn_{1.5}Ni_{0.5}O_4$ exhibits a good Li-ion diffusion coefficient at room temperature and good stability upon cycling even at 1 *C* charge–discharge rate. The discharge capacity of the $LiMn_{1.425}Ni_{0.525}Nb_{0.05}O_4$ still remains near 100% of original values even after 100 cycles. Our obtained results demonstrate that a small amount of Nb substitution in $LiMn_{1.5}Ni_{0.5}O_4$ can improve the rate cycling performance of this positive-electrode material, making it more attractive for future practical application.

## Acknowledgments

This work was financially supported by the National Natural Science Foundation of China (no. 50902001), the Key project of Scientific Research Foundation sponsored by Education Department of Anhui Province, China (no. KJ2010A045), and the Foundation for Young Talents in College of Anhui Province, China (no. 2010SQRL033ZD). The work is also supported by the Program for Innovative Research Team in Anhui University of Technology(no. TD201202).

## References

[1] F. Cheng, H. Wang, Z. Zhu, Y. Wang, T. Zhang, Z. Tao, J. Chen, Energy Environ. Sci. 4 (2011) 3668–3675.
[2] X. Ma, B. Kang, G. Ceder, J. Electrochem. Soc. 157 (2010) A925–A931.
[3] K. Amine, H. Tukamoto, H. Yasuda, Y. Fujita. Extended Abstracts 95-2. In: Electrochemical Society Fall Meeting 1995, Chicago, Abstract no. 70. p. 114.
[4] Q.M. Zhong, A. Bonakdarpour, M.J. Zhang, Y. Gao, J.R. Dahn, J. Electrochem. Soc. 144 (1997) 205–213.
[5] T. Ohzuku, S. Takeda, M. Iwanaga, J. Power Sources 81-82 (1999) 90–94.
[6] G.Q. Liu, L. Wen, Y.M. Liu, J. Solid State Electrochem. 14 (2010) 2191–2202.
[7] T.-F. Yi, Y. Xie, M.-F. Ye, L.-J. Jiang, R.-S. Zhu, Y.-R. Zhu, Ionics 17 (2011) 383–389.
[8] H.M. Wu, J.P. Tu, Y.F. Yuan, Y. Li, X.B. Zhao, G.S. Cao, Electrochim. Acta 50 (2005) 4104–4108.
[9] F.G.B. Ooms, E.M. Kelder, J. Schoonman, M. Wagemaker, F.M. Mulder, Solid State Ionics 152–153 (2002) 143–153.
[10] C. Locati, U. Lafont, L. Simonin, F. Ooms, E.M. Kelder, J. Power Sources 174 (2007) 847–851.
[11] S.B. Park, W.S. Eom, W.I. Cho, H. Jang, J. Power Sources 159 (2006) 679–684.

[12] M. Aklalouch, J.M. Amarilla, R.M. Rojas, I. Saadoune, J.M. Rojo, Electrochem. Commun. 12 (2010) 548–552.
[13] D. Li, A. Ito, K. Kobayakawa, H. Noguchi, Y. Sato, J. Power Sources 161 (2006) 1241–1246.
[14] R. Alcantara, M. Jaraba, P. Lavela, J.M. Lloris, C.P. Vicente, J.L. Tiradoz, J. Electrochem. Soc. 152 (2005) A13–A18.
[15] J.-H. Kim, S.-T. Myung, C.S. Yoon, I.-H. Oh, Y.-K. Sun, J. Electrochem. Soc. 151 (2004) A1911–A1918.
[16] T. Noguchi, I. Yamazaki, T. Numata, M. Shirakata, J. Power Sources 174 (2007) 359–365.
[17] S.H. Oh, K.Y. Chung, S.H. Jeon, C.S. Kim, W.I. Cho, B.W. Cho, J. Alloys Compd. 469 (2009) 244–250.
[18] H. Wang, H. Xia, M.O. Lai, L. Lu, Electrochem. Commun. 11 (2009) 1539–1542.
[19] H.S. Fang, Z.X. Wang, X.H. Li, H.J. Guo, W.J. Peng, J. Power Sources 153 (2006) 174–176.
[20] H. Liu, Y.P. Wu, E. Rahm, R. Holze, H.Q. Wu, J. Solid State Electrochem. 8 (2004) 450–466.
[21] Y. Sun, Y. Yang, X. Zhao, H. Shao, Electrochim. Acta 56 (2011) 5934–5939.
[22] J.-H. Kim, S.-T. Myung, Y.-K. Sun, Electrochim. Acta 49 (2004) 219–227.
[23] T.-F. Yi, Y. Xie, J. Shu, Z. Wang, C.-B. Yue, R.-S. Zhu, H.-B. Qiao, J. Electrochem. Soc. 158 (2011) A266–A274.
[24] M. Ganesan, S. Sundararajan, M.V.T. Dhananjeyan, K.B. Sarangapani, N.G. Renganathan, Mater. Sci. Eng. B 131 (2006) 203–209.
[25] Hui Xia, S.B. Tang, L. Lu, J. Alloys Compd. 449 (2008) 296–299.
[26] G. Ting-Kuo Fey, Y.D. Cho, T. Prem Kumar, Mater. Chem. Phys. 87 (2004) 275–284.
[27] T.-F. Yi, C.-L. Hao, C.-B. Yue, R.-S. Zhu, J. Shu, Synth. Met. 159 (2009) 1255–1260.
[28] K. Amine, H. Tukamoto, H. Yasuda, Y. Fujita, J. Electrochem. Soc. 143 (1996) 1607–1613.
[29] R.D. Shannon, Acta Crystallogr. A32 (1976) 751–767.
[30] T. Ohzuku, K. Ariyoshi, S. Takeda, Y. Sakai, Electrochim. Acta 46 (2001) 2327–2336.
[31] T. Yang, N. Zhang, Y. Lang, K. Sun, Electrochim. Acta 56 (2011) 4058–4064.
[32] B. Markovsky, Y. Talyossef, G. Salitra, D. Aurbach, H.-J. Kim, S. Choi, Electrochem. Commun. 6 (2004) 821–826.
[33] Q.-C. Zhuang, T. Wei, L.-L. Du, Y.-L. Cui, L. Fang, S.-G. Sun, J. Phys. Chem. C 114 (2010) 8614–8621.
[34] J. Liu, A. Manthiram, Chem. Mater. 21 (2009) 1695–1707.
[35] A.Y. Shenouda, H.K. Liu, J. Power Sources 185 (2008) 1386–1391.
[36] Q. Cao, H.P. Zhang, G.J. Wang, Q. Xia, Y.P. Wu, H.Q. Wu, Electrochem. Commun. 9 (2007) 1228–1232.
[37] C.Z. Lu, G. Ting-Kuo Fey, J. Phys. Chem. Solids 67 (2006) 756–761.
[38] R. Santhanam, B. Rambabu, J. Power Sources 195 (2010) 4313–4317.
[39] T.-F. Yi, J. Shu, Y.-R. Zhu, A.-N. Zhou, R.-S. Zhu, Electrochem. Commun. 11 (2009) 91–94.